ACS ENGINEERING Au
AN OPEN ACCESS JOURNAL OF THE AMERICAN CHEMICAL SOCIETY

Editors' Choice
Open Access

pubs.acs.org/engineeringau

Article

Tailored Platinum Group Metal/Spinel Oxide Catalysts for Dynamically Enhanced Methane Oxidation

Published as part of ACS Engineering Au virtual special issue "Materials Design".

Pak Wing Chen,[⊥] Debtanu Maiti,[⊥] Ru-Fen Liu, Lars C. Grabow,* and Michael P. Harold*

Cite This: *ACS Eng. Au* 2024, 4, 193–203

Read Online

ACCESS | Metrics & More | Article Recommendations | Supporting Information

ABSTRACT: A combined experimental and molecular modeling study identifies a family of spinel oxides that in combination with PGM (platinum group metals) provide enhanced methane oxidation activity. With a reduction in greenhouse gas (GHG) emissions urgently needed, there is renewed interest in the use of natural gas vehicles (NGVs) and engines (NGEs) for transportation, commerce, and industrial applications. NGVs and NGEs emit less CO_2 than their petroleum-derived counterparts but may emit uncombusted methane, an even more potent GHG. For stoichiometric engines, methane oxidation catalysts containing PGM and spinel oxide in layered architectures offer increased methane oxidation activity and lower light-off temperatures (T_{50}). The reducible spinel oxide has direct and indirect roles that are effectively described by the bulk oxygen vacancy formation energy (E_{vac}). We apply density functional theory (DFT) to identify several earth-abundant, cobalt-rich spinel oxides with favorable E_{vac}, shown to correlate with dynamic oxygen storage capacity (DOSC) and CO and H_2 oxidation activity. We experimentally rank-order the DFT-identified spinel oxides in combination with Pt+Pd for their methane oxidation activity measurements, under both time-invariant and modulated feed conditions. We show good agreement between the activity and the DFT-computed reducibility of the spinel oxide. The findings suggest spinel reducibility is a key factor in achieving enhanced low-temperature methane conversion, enabled through a balance of methane activation on the PGM sites and subsequent oxidation of the intermediates and byproducts on spinel oxides. In agreement with its computationally predicted E_{vac}, $NiCo_2O_4$ was confirmed to have the highest DOSC and lowest T_{50} among the tested spinel samples.

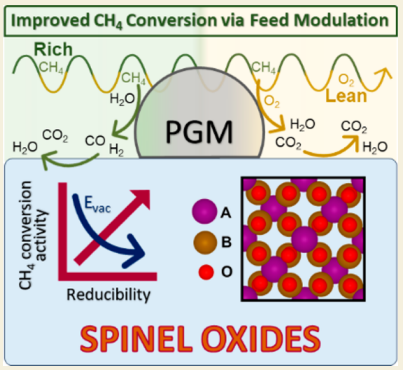

KEYWORDS: *spinel oxides, precious metal catalysts, dynamic oxygen storage, automotive catalysis, CH_4 conversion*

1. INTRODUCTION

The current energy and environmental landscape calls for reductions in greenhouse gas (GHG) emissions while improving energy utilization. Vehicles and stationary combustion engines remain a significant source of GHG, but domestic natural gas (NG) with its higher H:C ratio compared to petroleum-derived fuels is an attractive fuel replacement with reduced CO_2 generation.[1] Engines that utilize lean NG combustion are more efficient in terms of fuel economy than the stoichiometric NG combustion counterparts, but their emission control systems require advanced lean NO_x (x = 1,2) reduction. In contrast, stoichiometric engine emission control can use modified three-way catalyst (TWC) technology for NO_x reduction and abatement, which reduces the cost and complexity of the aftertreatment system.[2] Regardless of lean or stoichiometric operation, both combustion types emit unreacted methane (CH_4), which necessitates the development of advanced methane emission technology. While not an ozone precursor, methane is a potent GHG, with a warming potential about 25 times higher than that of CO_2. Motivated by the lower cost and lower complexity, we focus on stoichiometric methane emission control, where the challenge is to ensure high CH_4 conversion while keeping O_2 concentration sufficiently low to enable NO_x reduction.[2] Complicating matters is the need to meet emission targets under such typical dynamically changing conditions associated with the onboard control of the air/fuel (lambda) ratio, with fluctuation frequency as rapid as ∼1 Hz.

Catalysts used to remove pollutants from the exhaust of stoichiometric NG vehicles and engines are derived from the TWC, which contains a mixture of platinum group metals (PGM) combined with an oxygen storage material (OSM). The OSM enables an effective lambda under the dynamic conditions while achieving high conversion of three criteria pollutants; namely, nonmethane hydrocarbons (NMHCs), CO

Received: September 3, 2023
Revised: November 20, 2023
Accepted: November 21, 2023
Published: December 23, 2023

and NO_x.[3] The TWC has evolved over the years to meet the increasingly stringent emission levels for these pollutants. With methane being the main hydrocarbon constituent of NG, the TWC essentially must become a "four-way" catalyst (FWC) with methane added to the list of three. Higher PGM loading and metallic monolith substrates are typically employed to oxidize methane, which is the least reactive hydrocarbon. However, this is problematic due to the high cost of the precious metals. A looming challenge is to move toward cheaper earth-abundant elements while meeting the requisite light-off temperature and methane emissions targets.

Recent work by our group introduced new concepts for stoichiometric methane oxidation. We have shown that the combination of lean-rich modulation and spinel oxide addition to the PGM catalyst enhances the activity of methane oxidation catalysts.[4−6] Spinel oxides have the general formula AB_2O_4 (A, B = metal) and are known as materials with high oxygen storage capacity (OSC).[7] Chen et al.[6] reported enhanced methane light-off, with a ∼85 °C temperature reduction at 50% methane conversion (T_{50}), under lean-rich modulation over a $Pt+Pd/Al_2O_3$ monolith with $Mn_{0.5}Fe_{2.5}O_4$ spinel addition. The PGM and spinel components are present as two washcoat layers in a dual-layer design with PGM in the top layer. The spinel addition also reduces the required PGM loading in the catalyst formulation.[4,7] This is in line with earlier work from Golden et al.,[7] who reported that the incorporation of the Cu−Mn based spinel in a Pd based TWC allows for improved catalyst activity in NO_x and hydrocarbons removal.

The benefit of adding spinel to PGM catalysts has multiple origins. Direct activation and oxidation of CH_4 on spinel oxides is possible, but only at temperatures above 500 °C.[4−6] Thus, the observed reduction in the light-off temperature for CH_4 oxidation below 500 °C cannot be attributed to a direct role of spinel. More likely explanations for the improved CH_4 light-off activity of PGM/spinel catalysts assign an indirect role to spinel that leverages their reducibility, or dynamic oxygen storage capacity (DOSC), working synergistically with PGM layers under dynamic conditions.[5] The basic function of the spinel is to serve as the OSM to store and release oxygen, while the primary function of the PGM is to catalyze the methane oxidation and reforming chemistries. During the switch from a net lean to a net rich feed, a noted enhancement in the methane conversion rate is encountered. This appears to be due to the direct involvement of the spinel in the conversion (oxidation) of the methane partial oxidation and steam reforming products CO and H_2, which are shown to inhibit methane reforming. Their removal under modulation is key to sustaining a higher methane consumption rate.

With FWCs being derived from TWCs, viable strategies to further improve their low temperature activity and to reduce their PGM loading can mirror those used for TWCs. The TWC performance under lean/rich cyclic feed conditions is found to be closely related to the oxygen storage and release function of the OSM. Heo et al.[8] have attributed the catalyst activity loss of a Pd based TWC to not only the sintering of Pd, but also the gradual loss of OSC of the catalyst. Bickel et al.[9] have reported that the OSC can be used as a property for rapid screening of catalysts. It has been shown that the OSM can play an important role in catalyst activity. Thus, a strategy to improve the catalyst activity is to optimize the composition of the OSM with a focus on CH_4 activation under stochiometric conditions with lean/rich modulation.

Oxygen storage capacity can be divided into two categories: the total OSC and the dynamic oxygen storage capacity (DOSC). The former is the "limiting" amount of transferable oxygen including surface and bulk oxygen that can be obtained by prolonged reduction at a given temperature. This amount represents the maximum reducibility of the OSM. DOSC is the more application relevant property as it is a measure of the amount of the surface oxygen transferred under the fast oxidant/reductant pulses simulating the lean/rich modulation in the exhaust gas.[10,11] OSC and DOSC are influenced by various factors, such as the nature of the reducing agent, the concentration of the reductants, and temperature. Zhou et al.[12] conducted DOSC measurements of the $Mn_{0.5}Fe_{2.5}O_4$ (MFO) spinel using fast lean-rich cycling (0.5−2 Hz) with CO as a reductant and found that only oxygen near the MFO crystal surface is consumed, with diffusion of bulk oxygen playing a minor role. In a later study, Zhou et al.[13] developed a DOSC kinetic model that accounts for the fast reduction/reoxidation step of spinel during the lean-rich cycles. The reduction of MFO spinel with CO was found to be slower than its subsequent reoxidation by O_2. Similarly, Yao et al.[10] reported that the reoxidation of reduced ceria is a rapid process, which occurs at temperatures as low as room temperature. Thus, the reduction step or reducibility of spinel determines the transient DOSC performance and therefore is an informative property for screening spinel materials.

Because spinel oxides exist in many compositions and degrees of inversion, they have highly tunable properties; yet, they are sparsely explored candidates as an OSM in emissions treatment. Fino et al.[14] evaluated a subset of spinels (AB_2O_4, A= Co, Mn, Mg; B= Cr, Fe) combined with PGM in terms of T_{50} (CH_4 light-off temperature at 50% CH_4 conversion) for CH_4 oxidation in lean NG vehicle exhaust gas treatment. The Pd-doped $CoCrO_4$ spinel catalyst was identified to be the most active, with the lowest T_{50} of 321 °C. Similar studies of CH_4 activation on complex dual-layer catalysts of industrial merit under relevant stoichiometric conditions have not yet been reported.

In this work, we examine the direct and indirect roles of spinel oxides during PGM-catalyzed CH_4 conversion under stoichiometric conditions, with the aim to converge on dual-layer catalyst formulations that lower CH_4 light-off temperatures. To this end, we employ a computational screening approach of AB_2O_4 spinels with earth-abundant metals (A, B = Mn, Fe, Co, Ni) using the binding energy of hydrogen (B.E.(H)) and the oxygen vacancy formation energy (E_{vac}) as descriptors. The hydrogen affinity of oxides is a good indicator for their ability to catalyze C−H bond scission,[15,16] while E_{vac} approximates the ease of oxygen removal from the spinel oxide lattice. One of most prominent OSMs, ceria (CeO_2), is known to oxidize CO via a Mars−van Krevelen-type mechanism.[17,18] Hence, E_{vac} is expected to correlate not only with reducibility and DOSC, but also with CO and H_2 oxidation activity, as long as Mars−van Krevelen-type mechanisms prevail. Our computational predictions identify Co-rich spinels as the most promising subset, corroborated by experimental studies of catalyst performance and DOSC measurements.

2. EXPERIMENTAL SECTION

2.1. Monolith Catalysts

All of the monolith catalysts used in the study were provided by CDTi Advanced Materials, Inc. (Oxnard, CA); their compositions and

https://doi.org/10.1021/acsengineeringau.3c00053
ACS Eng. Au 2024, 4, 193−203

architectures are provided in Table 1. Each of the samples have the same dimension of 1 in. (D) and 0.85 in. (L) and the same 600 cpsi (cells per square inch) cordierite substrate.

Table 1. Summary of Monolith Catalysts

Monolith catalysts	Architecture	PGM loading (g/ft^3)	Spinel loading (g/L)
PGM-Only	PGM top layer (100 g/L)	30[a]	0
PGM-Only2	Al_2O_3 bottom layer (60, 100 g/L)		
Spinel-Only	Spinel layer (60 g/L)	0	15[b]
PGM+Spinel	PGM top layer (100 g/L)	30[a]	15[b],10[c]
PGM+Co-Spinel	Spinel bottom layer (60, 100 g/L)		

[a]Pt:Pd-19:1/Al_2O_3 [b]$Mn_{0.5}Fe_{2.5}O_4$ spinel layer (60 g/L) composition: 25 wt % spinel/75 wt % Al_2O_3 [c]Cobalt based spinel layer (100 g/L) composition: 10 wt % spinel/90 wt % Al_2O_3

Figure 1a shows a schematic of three different types of monolith samples. The "PGM+Spinel" and "PGM-Only" catalysts have a dual-layer structure with a top layer of Pt+Pd/Al_2O_3 and a bottom layer of spinel/Al_2O_3 or Al_2O_3. The "Spinel-Only" catalyst has a single layer of spinel/Al_2O_3. For all the samples, the PGM layer has a washcoat loading of 100 g/L monolith and a composition of 1 wt % of PGM (19:1 wt ratio of Pt and Pd) supported on Al_2O_3 with an overall metal loading of 30 g PGM/ft^3. Both the spinel and Al_2O_3 layers have loadings of 60 g/L monolith. The spinel layer contains dispersed $Mn_{0.5}Fe_{2.5}O_4$ with a mass fraction of 25 wt % on Al_2O_3. To verify the performance of DFT-predicted Co spinels, a separate set of monolith catalysts shown in Figure 1b was used. The "PGM+Co-Spinel" and "PGM-Only2" have the same PGM top layer as the PGM+Spinel and PGM-Only catalysts, but the bottom spinel or Al_2O_3 layer has a higher washcoat loading of 100 g/L monolith. The spinel layer contains dispersed cobalt-based spinel with a lower mass fraction of 10 wt % on Al_2O_3.

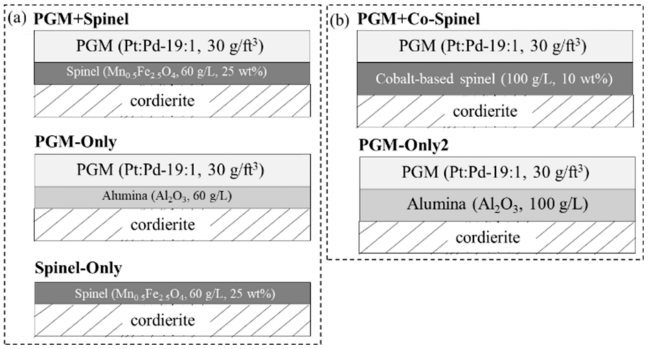

Figure 1. (a) Three types of washcoated monolith samples with varying spinel loadings [PGM layer thickness: 1.64 g/in^3; spinel layer thickness: 0.98 g/in^3]; (b) two types of washcoated monolith samples [PGM and spinel layer thickness: 1.64 g/in^3].

2.2. Powder Catalysts

Powder samples including $NiCo_2O_4$, $Fe_{0.5}Co_{2.5}O_4$, and $MnCo_2O_4$ were also provided by CDTi Advanced Materials, Inc. (Oxnard, CA). All samples have the same spinel mass fraction of 15 wt % on γ-Al_2O_3 support.

2.3. Flow Reactor Experiments

The catalyst performance tests were conducted in the same bench reactor system described in our previous work.[4] An application-relevant "full" feed simulating the NGV exhaust gas was used, and the concentrations of each species are listed in Table 2. The concentration of each species is kept constant for the time-invariant feed condition, while for the modulated feed the O_2 concentration was cycled between a lower rich value ($\lambda < 1$) to a higher lean value ($\lambda > 1$) every 1.5 s, corresponding to a lean/rich cycle of 3 s and a frequency of 0.33 Hz. The parameter lambda (λ) is defined by

Table 2. Feed Compositions Used in This Study

Species[a]	Full feed, time-invariant λ = 0.992	Full feed, modulated λ_{avg} = 0.992 (0.978−1.006 at 0.33 Hz)
CH_4	1500 ppm	1500 ppm
CO	8000 ppm	8000 ppm
H_2	1000 ppm	1000 ppm
NO	1000 ppm	1000 ppm
O_2	5650 ppm	3400−7900 ppm
H_2O	10%	10%
CO_2	10%	10%

[a]N_2 balance

$$\lambda = \frac{0.5[(CO) + 2(O_2) + (NO) + (H_2O) + 2(CO_2)]}{[(CO) + (CH_4) + (CO_2)] + 0.25[2(H_2) + 4(CH_4) + 2(H_2O)]} \quad (1)$$

and is used to characterize the lean/rich ratio of the time-invariant (λ = 0.992) and modulated full feed (λ = 0.978−1.006).

The gas hourly space velocity (GHSV) was set at 40,000 h^{-1} (@ STP), corresponding to a total volumetric flow rate of 7.2 standard L/min for all the flow experiments. The outlet concentrations of CH_4, CO, CO_2, H_2O, and NO were measured by a FTIR (MKS MultiGas 2030) and the H_2 concentration was measured by a mass spectrometer (MKS Cirrus 1). The full feed experiments were conducted with a fixed temperature ramp rate at 5 °C/min from 105 to 600 °C. The temperature readings reported were measured by an inlet thermocouple fixed at the position of 5 mm away from the catalyst.

Before each experiment, the monolith samples were pretreated at 550 °C for 30 min in 3% O_2 in balance N_2 to remove air and moisture in the reactor system.

Caution! *This procedure requires the use of methane, hydrogen, carbon monoxide, oxygen, and nitric oxide gases. methane, hydrogen, and carbon monoxide are classified as GHS flammable gas, Category 1. Oxygen and nitric oxide are classified as GHS oxidizing gas, Category 1. The storage and use of the compressed gas cylinders were handled using standard OSHA procedures.*

2.4. X-ray Powder Diffraction

The powder X-ray diffraction (XRD) patterns of the cobalt-based spinel powder samples $NiCo_2O_4/Al_2O_3$, $Fe_{0.5}Co_{2.5}O_4/Al_2O_3$ and $MnCo_2O_4/Al_2O_3$ were measured using an Empyrean Malvern analytical diffractometer (40 kV, 40 mA) with a Cu Kα X-ray source (λ = 1.54 Å). The diffraction patterns were collected for a range of 10° to 70° with a step size of 0.02°.

2.5. Specific Surface Area Quantification of Powder Spinel Samples

The specific surface area is measured by Brunauer−Emmett−Teller (BET) analysis performed on a Micromeritics TriStar II unit using the nitrogen isotherm gas adsorption method.

2.6. Dynamic Oxygen Storage Capacity Quantification

The DOSC measurements were conducted in a fixed bed reactor, described in detail elsewhere.[12] The experiments were conducted with reduction/oxidation cycle, which involved a 60 s reduction period (1% CO/Ar), 60 s Ar flow, 60 s oxidation period (0.5% O_2/Ar) and 60 s Ar flow. An illustration of the reduction−oxidation cycles is shown in Figure 2. The cycle was repeated at each temperature. A total flow rate of 150 sccm was used throughout the study. The outlet concentrations of CO, CO_2 and O_2 were measured by a mass spectrometer (Hiden Analytical, HPR20). The experiments were conducted at temperatures between 350 to 600 °C. The temperature

https://doi.org/10.1021/acsengineeringau.3c00053
ACS Eng. Au 2024, 4, 193−203

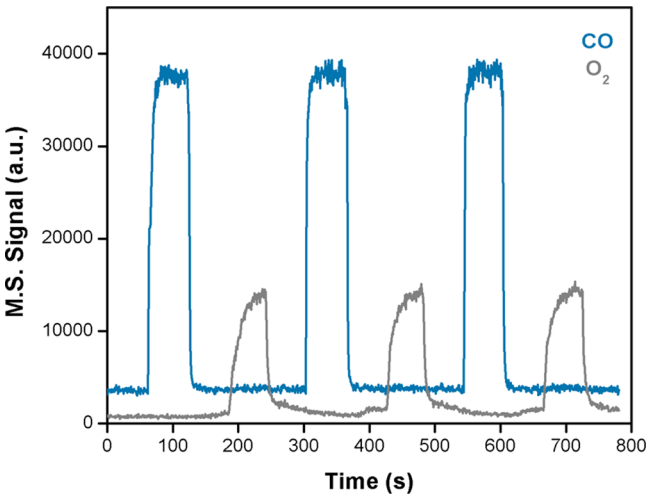

Figure 2. Illustration of CO reduction (60 s) - O_2 oxidation (60 s) cycles over spinel in DOSC measurements.

readings reported are averaged temperature readings measured by two thermocouples placed upstream and downstream of the catalyst bed.

For each experiment, 15 mg of catalyst sample (mesh size 40 to 60) was first mixed with 150 mg of quartz sand of the same mesh size. The addition of quartz sand ensured a uniform temperature profile along the catalyst bed. Before every experiment, the catalyst was pretreated at 550 °C for 30 min in Ar and then cooled to 50 °C in Ar to remove the air and moisture present in the reactor tube. The DOSC value was determined according to

$$\mathrm{DOSC}\left[\frac{\text{mol O}}{\text{mol OSM}}\right] = \frac{N_{CO_2,\text{formed}}}{N_{\text{OSM}}} \tag{2}$$

The amount of CO_2 generated during each reduction period was quantified, and the reported DOSC values were the average quantity.

3. COMPUTATIONAL METHODOLOGY

As depicted in Figure 3, spinel oxides of composition AB_2O_4 (such as $MnFe_2O_4$), can exhibit a normal phase where all of

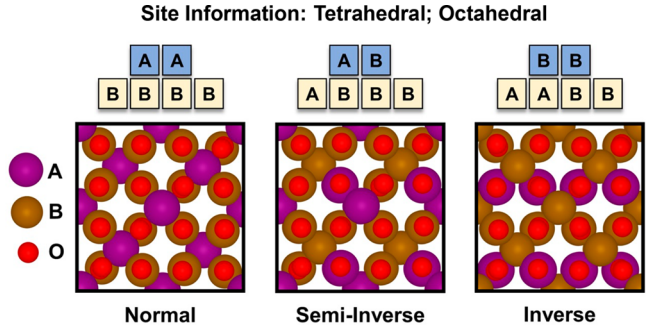

Figure 3. Representative structures of normal, semi-inverse and inverse phases of AB_2O_4 type spinel oxides. A normal phase comprises tetrahedrally coordinated A metals, while all the B metals are in octahedral sites. Inverse phase exhibits an opposite pattern, and the semi-inverse phases have a blend of A and B metals in both types of sites.

the A (Mn) atoms are in the tetrahedral coordination sites, and all of the B (Fe) atoms are in the octahedral sites. A contrasting inverse phase happens when all the A (Mn) atoms are in the octahedral sites, while the B element (Fe) reside in the available octahedral and tetrahedral coordination sites. A range of partially inverted phases with some A atoms in octahedral sites may also exist. It is worth noting that further variations in these materials are possible due to different spin states exhibited by the transition metals in the tetrahedral and octahedral sites. With all these crystallographic variations, spinel oxides can exhibit a vast range of electronic and chemical characteristics.

Spinel oxides of different phases (Figure 3) and compositions were probed via periodic density functional theory calculations using the Vienna ab initio simulation package (VASP).[19−23] The composition space comprises transition metals Mn, Fe, Co, and Ni. Since these transition metal oxides have localized electrons, we used a Hubbard U parameter of 3.3 eV for the "*d*" orbitals throughout our calculations. As reported by Wang et al., a Hubbard U value of 3.3 eV can be used to predict reliable oxidation energies of Mn, Fe, and Co based metal oxides within the GGA+U framework.[24] Exchange and correlation between valence electrons were described using the BEEF-vdW functional with an energy cutoff of 600 eV.[25] We used the $Fd\bar{3}m$ primitive crystal lattice for the spinel systems comprising six metal atoms and eight oxygen atoms. A gamma centric 8 × 8 × 8 k-point mesh was used for all calculations, and convergence was verified. Lattice constants for the stoichiometric AB_2O_4 bulk materials were obtained through optimization using the Birch−Murnaghan equation of state. The stable spin configurations for each of the normal, inverse, and semi-inverse spinel phases were identified by calculating the energies of different spin configurations, including high spin ferromagnetic states, and a range of ferrimagnetic states arising from antiparallel magnetic moments in the tetrahedral and octahedral sites. Bader charge analysis was performed to assign partial charges.[26,27] The charge reported for the lattice oxygen in each spinel is the average across all oxygen atoms. Oxygen vacancy formation energies (E_{vac}) were calculated for each lattice oxygen sites as per the following equation, and the reported E_{vac} is an average across all the lattice oxygen atoms.

$$E_{\text{vac}} = E_{\text{vacant\_spinel}} - E_{\text{stoic\_spinel}} + \frac{1}{2}E_{O_{2(g)}} \tag{3}$$

In eq 3 $E_{\text{vacant\_spinel}}$ is the energy of bulk spinel oxide with an oxygen vacancy, $E_{\text{stoic\_spinel}}$ is the energy of the pure stoichiometric spinel oxide, and $E_{O_{2\,(g)}}$ is the energy of gas phase oxygen, which was adjusted from its DFT calculated value to match the tabulated heat of formation of H_2O.

The binding energy of hydrogen, B.E.(H), on each bulk lattice oxygen atom is defined as

$$\text{B.E.(H)} = E_{\text{spinel+H}} - E_{\text{stoic\_spinel}} - \frac{1}{2}E_{H_{2(g)}} \tag{4}$$

where $E_{\text{spinel+H}}$ is the energy of the H-bonded spinel system and $E_{H_{2\,(g)}}$ is the energy of gas phase hydrogen. We have reported the average B.E.(H) per spinel phase averaged across all lattice oxygens in the spinel structure. The average *d* electron content of the spinel oxides is reported as $\sum_i w_i d_i$, where w_i is the fractional occupation of cation sites by metal *i*, with a *d* electron filling of d_i.

4. RESULTS AND DISCUSSION

4.1. CH_4 Conversion on PGM-Spinel Dual-Layer Catalyst

The effect of the MFO spinel oxide on the CH_4 light-off temperatures under conditions simulating NGV exhaust are shown in Figure 4. Under both modulated and time-invariant

https://doi.org/10.1021/acsengineeringau.3c00053
ACS Eng. Au 2024, 4, 193−203

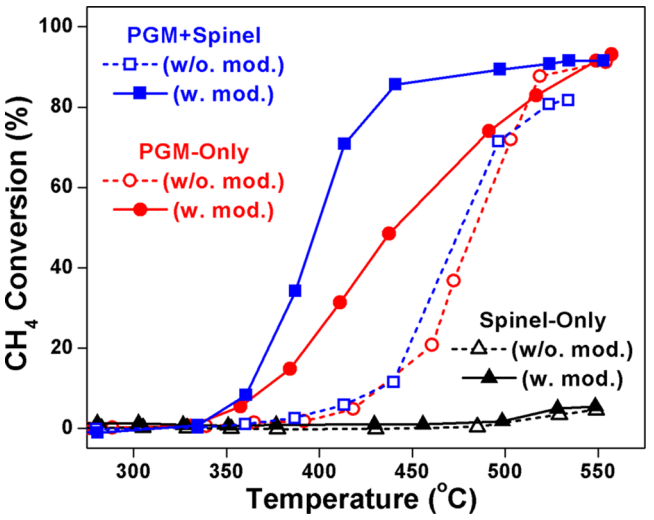

Figure 4. CH_4 conversion under modulated [filled symbols] and time-invariant [open symbols] feeds.

feed conditions, the presence of spinel in the PGM+Spinel catalyst lowers the CH_4 light-off temperature, as defined by the temperature at 50% CH_4 conversion (T_{50}). The Spinel-Only catalyst is only capable of converting methane at temperatures exceeding ≥500 °C for both feed conditions. In contrast, the T_{50} for the PGM-Only catalyst is 488 °C. Further, under lean/rich cycling, some methane conversion enhancement (50 °C reduction in T_{50}) is observed. However, the cycling enhancement is less than that observed for the sample containing spinel. This result reveals an interesting promoting role of the spinel oxide during feed modulation under these application-relevant NGV-exhaust conditions.

The simplest explanation for the greater cycling enhancement in the presence of spinel can be provided by drawing an analogy to ceria. Ceria possesses high OSC, allowing it to be partially reduced under rich conditions and, in turn, storing excess oxygen under lean conditions. The presence of CeO_2 or spinel as an oxygen buffer lowers the oxygen coverage on Pt. This benefits CH_4 oxidation, because when the Pt surface is partially covered by oxygen, DFT studies by Chin et al.[28] identified pairs of exposed Pt sites and oxygen adatoms as favorable activation sites, but with increasing O_2 pressure, the CH_4 oxidation rate over Pt/Al_2O_3 decreases due to O_2 inhibition by site blocking. Compared to the Pt/Al_2O_3 catalyst, Pt/CeO_2 is less sensitive to O_2 inhibition and maintains higher CH_4 oxidation activity, particularly during modulated lean/rich operation.[29] While oxygen storage is an important function provided by the spinel, it serves additional roles in dynamic methane oxidation.

Figure 5 shows the reactor effluent concentration data for the other feed constituents (CO, H_2) over the PGM-Only catalyst (Figure 5a) and PGM+Spinel catalyst (Figure 5b), under time-invariant and modulated feed conditions. Even before CH_4 conversion commences (Figure 4), CO and H_2 are completely consumed. Under both feed conditions, both H_2 and CO are consumed at 280 °C over the PGM+Spinel catalyst. For the PGM-Only catalyst, CO and H_2 deplete at somewhat higher temperature; i.e. 330 °C (modulated feed) and at 340 °C (time-invariant feed). For both catalysts, the observed decrease in CO and H_2 conversions (increase in effluent concentrations) at high temperature under both feed conditions (>400 °C under modulated feed and >475 °C

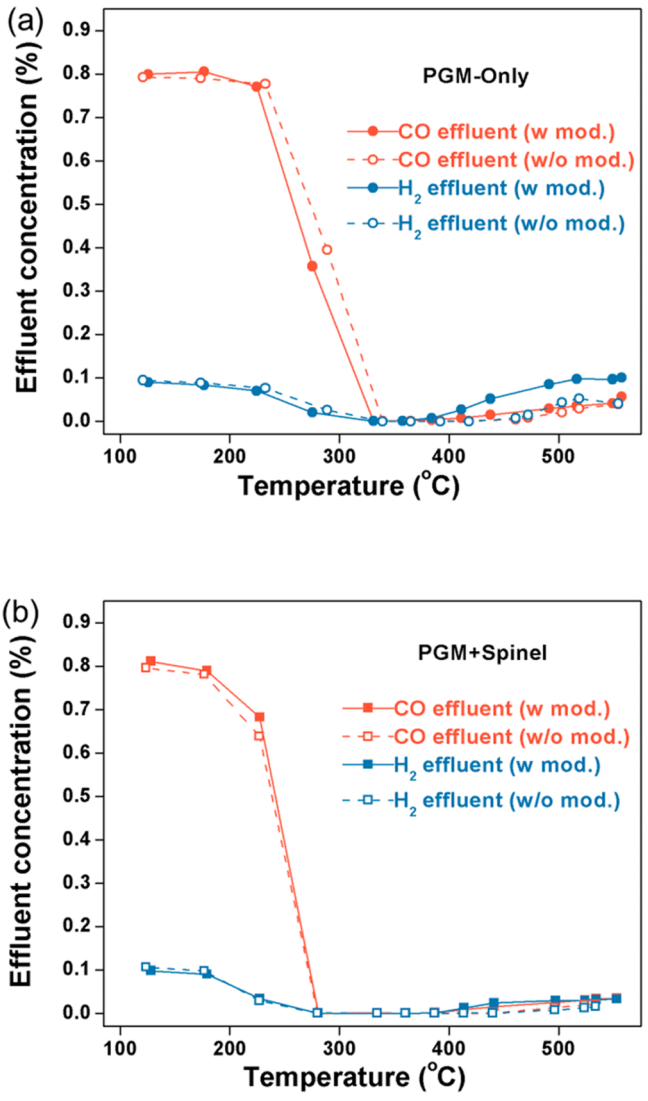

Figure 5. Effluent data for CO and H_2 over (a) the PGM-Only catalyst and (b) the PGM+Spinel catalyst under modulated [filled symbols] and time-invariant [open symbols] feeds.

under time-invariant feed) is attributed to steam methane reforming (SMR), not methane partial oxidation. Our previous study has provided detailed discussions on the effluent O_2 profiles and demonstrated that depletion of O_2 occurs at about the same temperature at which CO and H_2 formation commence.[6] A detailed discussion on the separate role of feed modulation and spinel oxide on the enhancement of CH_4 oxidation was discussed previously.[4−6]

For the spinel-containing catalyst, the depletion of H_2 and CO occurs at a somewhat lower temperature because the spinel provides additional activity for CO and H_2 oxidation. Similarly, the rates of CO and H_2 formation are higher at ∼550 °C for the PGM-Only catalyst compared to the PGM+Spinel catalyst under the modulated feed condition (Figures 5a,b). Without spinel, the reductants are not removed by oxidation. CO-TPR, H_2-TPR and CH_4-TPR data on spinel oxides reveal the role of spinel oxides. Zhou et al.[12] reported over the $Mn_{0.5}Fe_{2.5}O_4/Al_2O_3$ that CO and H_2 uptake starts at 150 °C. On the other hand, CH_4 uptake starts at the higher temperature of 350 °C (Figure S1). Thus, the enhanced

https://doi.org/10.1021/acsengineeringau.3c00053
ACS Eng. Au 2024, 4, 193−203

CH_4 conversion observed over the PGM+Spinel catalyst is not a result of direct CH_4 activation over the spinel oxide.

Based on the above experimental trends, we provide an explanation of the indirect role of spinel in CH_4 conversion enhancement. At low CH_4 conversion, spinel serves as an oxygen buffer, lessening the O_2 inhibition effect on CH_4 oxidation over PGM. Spinel oxides may be partially reduced under rich conditions and some of the excess gas phase oxygen under lean conditions is consumed by the partially reduced spinel. Despite its location in a separate, albeit contiguous, layer, spinel provides enhancement through gas phase O_2 diffusion to and removal by the MFO spinel layer, maintaining the PGM surface in a partially oxidized state for enhanced CH_4 activation. At high CH_4 conversion with depletion of gas phase O_2, CO and H_2 form via steam reforming. While spinel oxides lack methane oxidation activity at low temperatures (<500 °C), they are active for CO and H_2 oxidation. The presence of spinel oxides allows for the removal of CO and H_2, thus making more PGM sites available for CH_4 activation/dissociation. The removal of CO and H_2 by the oxygen storage function from spinel also drives the SMR activity, due to the inhibiting nature of CO and H_2 on SMR. (We report elsewhere the results of a comprehensive kinetics study of SMR on the same PGM in the current study.) This oxygen storage role of spinel oxides is not only critical for low-temperature CH_4 activation, but also allows for reduction of PGM content in TWC systems (Figure S2), motivating the search of better-performing spinel oxides for low temperature CH_4 conversion. As discussed above, the onset of CO oxidation by the MFO spinel is estimated to be above 400 °C after O_2 depletion under modulated feed condition. The onset of H_2 oxidation by spinel occurs at a similar temperature (Figure 5b). Thus, we hypothesize that new spinel candidates that can oxidize CO and H_2 under dynamic feed condition at lower temperatures may lead to improved catalyst performance in CH_4 conversion. Detailed discussion is provided in later sections.

4.2. Rational Design of Improved Spinel Oxides

Spinel oxides, like many mixed metal oxides, are excellent platforms for material property tuning. As described earlier, they are composed of a vast array of metal cations at two different coordination sites: tetrahedral and octahedral. Based on the location of the constituent metals at these different sites, spinels are known to exhibit varying inversion symmetry of the crystal phases. Here, we have studied spinel oxides with possible metal compositions as A_3O_4, $A_{0.5}B_{2.5}O_4$, and AB_2O_4, with Mn, Fe, Co, and Ni as earth-abundant constituents as deemed feasible for automotive applications.

In the context of CH_4 oxidation in combination with PGMs, spinel oxides serve either a direct or an indirect role. To describe differences in direct CH_4 activation over metal oxides, the binding energy of atomic hydrogen to lattice oxygen (B.E.(H)) serves as an effective descriptor because higher intrinsic hydrogen affinity can drive C−H bond dissociation of CH_4.[15] For mixed metal oxides, such as spinels, exposed lattice oxygen atoms vary in their catalytic properties and offer a distribution of binding sites for H with different behaviors.[30] Indirect roles of spinel include oxygen storage and the oxidation of CO and H_2 which are known to inhibit CH_4 steam reforming. These functionalities are all related to the reducibility of the material or, equivalently, its metal−oxygen bond strength, which can be approximated by the oxygen vacancy formation energy (E_{vac}). The reduction process is initiated by dissociation of surface metal−oxygen bonds and subsequent removal of the surface lattice oxygen atoms. A gradual bulk reduction follows due to the bulk-surface diffusion of oxygen atoms, which may be depleted at the surface. While the formation energy of an oxygen vacancy at the surface appears to be a more relevant catalytic descriptor, the large materials space studied here and the even larger number of possible exposed surface facets make it unfeasible to examine all possible exposed oxygen sites. Instead, we approximate the trends in reducibility and metal−oxygen bond strength from bulk calculations. Maiti et al.[31] have shown earlier that the trends of oxygen vacancy formation energies hold true across bulk and surfaces of perovskite oxides. We assert that for the purpose of computationally screening improved spinels for use in dual-layer PGM-spinel catalysts for methane activation, these averaged bulk values of the descriptors B.E.(H) and E_{vac} are expected to lead to meaningful predictions.

The descriptors B.E.(H) and E_{vac} for 64 spinel compositions within the considered material space are shown in Figure 6.

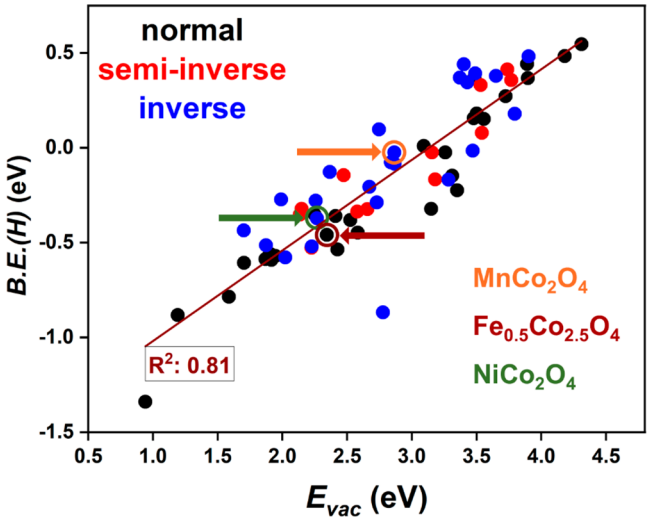

Figure 6. Linear relationship between binding energy of hydrogen, B.E.(H), and oxygen vacancy formation energy, E_{vac}, of normal, inverse, and semi-inverse phases of spinel oxides.

The linear correlation of these two descriptors is inherently embedded in the material chemistry of these materials. While E_{vac} is purely a depiction of ease of O-removal from a metal−oxygen bond, B.E.(H) describes the affinity of the oxygen atoms to attract/bind to H atoms. An O atom that is strongly bonded to the metal sites may be less available for H binding. Furthermore, it is energy-intensive to break free from that M-O bond. On the other hand, an O atom that presents favorable H binding portends to a weak M-O binding, thus exhibiting lower E_{vac}. This is critical in the sense that the activity of the spinels in two quite different chemical reactions (H binding and O vacancy formation) can be studied by one descriptor. Simply put, a reducibility descriptor, E_{vac}, can explain both reducibility and C−H activation trends on spinel oxides, as it was previously suggested for doped CeO_2.[16]

As is evident from Figure 6, the extent of reducibility varies by ca. 3.5 eV for the explored spinel compositions. When screening for promising candidates, two factors were considered: (i) stability of the spinel oxides under relevant reaction conditions and (ii) experimentally reported stable spinel phases. One of the main criterion for harnessing

https://doi.org/10.1021/acsengineeringau.3c00053
ACS Eng. Au 2024, 4, 193−203

sustained DOSC from spinel oxides under modulated feed conditions is their stability. Too low of an E_{vac} is indicative of a tendency to decompose under reducing conditions. The reported E_{vac} is referenced to the energy of gas phase O_2. If the spinel reduction is formulated with respect to a reductant, such as H_2 or CO, the vacancy formation energies will be lowered by the heat of reaction for H_2 or CO oxidation. The spinel-induced enhancement of methane light-off has been attributed in part to the oxidation of H_2. Thus, considering the reaction $H_2 + O^* \rightarrow H_2O$, the exothermic heat of formation of water (ca. −2.7 eV) would need to be added to the reported formation energies, rendering many of them negative. To balance stability with activity, we focus on materials with 2.25 eV < E_{vac} < 3 eV. This allows the identification of materials that are prone to facile reduction under H_2 and CO, but without requiring a high energy barrier for reoxidation (materials with E_{vac} < 2.25 eV). In other words, we focus on spinel compositions that are amenable to reversible oxygen vacancy formation—aligned with the concept of dynamic oxygen storage capacity. An upper limit of E_{vac} = 3 eV was chosen to eliminate spinel oxides suffering from limited reducibility, which includes our baseline material $Mn_{0.5}Fe_{2.5}O_4$ with an E_{vac} of 3.9 eV. This interval of 2.25 eV < E_{vac} < 3 eV leaves us with only 18 spinel candidates out of the 64 studied (detailed in Table S1).

The second aspect for spinel selection is the experimentally reported phases and their stability. In our previous work, we have reported that $Mn_{0.5}Fe_{2.5}O_4$ decomposition forms mobile Mn and Fe species, which tend to encapsulate the PGM.[6] To suppress this detrimental effect, we confined our spinel composition space to formulations with low concentrations of Mn and Fe. A close inspection of the remaining materials showed that several Co-rich spinels satisfy our criteria, and we decided to focus on this subset (10 candidates). Among the Co-rich spinel phases, we selected compositions that include one of the three remaining elements (Ni, Fe, and Mn), of which three could be synthesized: $NiCo_2O_4$, $Fe_{0.5}Co_{2.5}O_4$ and $MnCo_2O_4$. While we did not study the inversion symmetry exhibited by these compounds, we assumed those to match with the literature.[32−35] The DFT-calculated descriptors E_{vac} and B.E.(H) for these three samples are reported in Table 3

Table 3. DFT-Calculated Properties of Bulk Spinel Oxides

Spinel Oxides	E_{vac} (eV)	B.E.(H) (eV)
$MnCo_2O_4$	2.86	−0.02
$Fe_{0.5}Co_{2.5}O_4$	2.34	−0.46
$NiCo_2O_4$	2.26	−0.37

and marked in Figure 6. The reducibility of these spinel oxides reduces in the order $NiCo_2O_4$, > $Fe_{0.5}Co_{2.5}O_4$ > $MnCo_2O_4$. We note that all three bulk spinels are metastable and have a positive energy of formation with respect to their binary suboxides with identical oxidation states (Table S2). Nanoscale spinel crystallites on Al_2O_3 support, however, may have extended stability windows as reported for sodium oxides.[36] Thus, bulk thermodynamic stability is an inadequate descriptor of long-term durability. Moreover, we argue that metastability may be a necessary requirement for high-performance dynamic OSMs, because dynamic oxygen storage requires fast and reversible oxygen transfer, which would be inhibited by the presence of a thermodynamic sink.

4.3. Co-Rich Spinels for Low Temperature CH_4 Activation

The Co-rich spinels identified by DFT were prepared by incipient wetness impregnation, and the Al_2O_3 supported spinel oxide were washcoated for preparing the dual-layer PGM+Spinel catalysts. The XRD patterns of the cobalt-based spinel samples are shown in Figure 7. They reveal a cubic

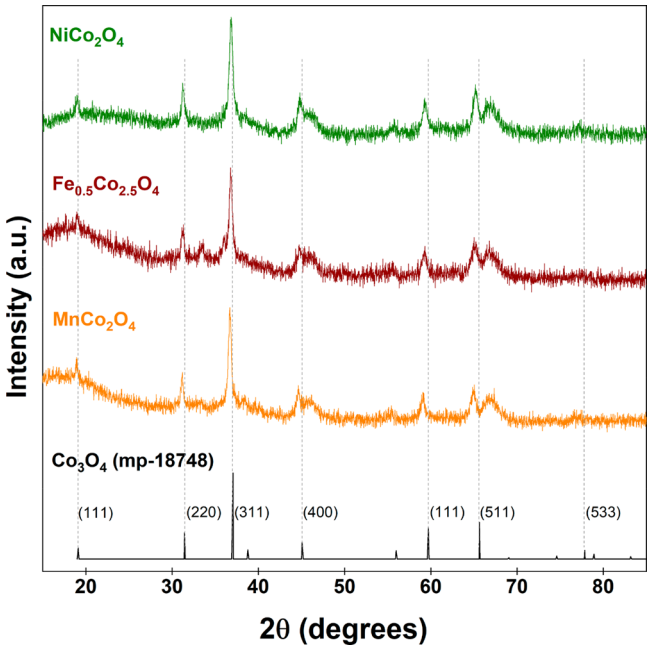

Figure 7. X-ray powder diffraction patterns for spinel oxides used in this study.

spinel structure like that of Co_3O_4 (Inorganic Crystal Structure Database (ICSD) card number 28158, also matching with material ID: mp-18748 from The Materials Project).[37] A slight shift of the XRD patterns for $MnCo_2O_4$, $Fe_{0.5}Co_{2.5}O_4$, and $NiCo_2O_4$ relative to that of Co_3O_4 marks the expansion of lattice due to Mn, Fe and Ni doping, respectively. No other secondary metal oxide phases were detected.

For quantifications of oxygen storage, previous studies on different OSMs (ceria-zirconia, spinel) used a pulse injection technique with CO, H_2, or small hydrocarbons as the reductant.[10,12,38,39] Several comparisons between ceria-zirconia (CZO) and spinels in terms of OSC and DOSC have been published. For instance, Golden et al.[7] reported that the Cu−Mn based spinel exhibits around 10 times higher OSC compared to CZO. Zhou et al.[12] quantified and compared the DOSC values of the MFO spinel and CZO. Using a pulse injection method with CO or C_3H_6 as the reductant, spinel has up to a 10× higher DOSC than CZO. Following the approach by Zhou et al., we conducted the DOSC experiments on the Co-rich spinel samples using the pulse injection method and CO was chosen as the reductant.

In addition to being a coreactant in the full feed, CO is also produced via CH_4 partial oxidation and reforming (after O_2 depletion). Thus, CO reduction was chosen to model the reduction of spinel. A total of 15 mg of 15 wt % spinel is used for each sample, thus yielding 9.35 μmol of $NiCo_2O_4$, 9.40 μmol of $Fe_{0.5}Co_{2.5}O_4$ and 9.50 μmol of $MnCo_2O_4$. The DOSC measurements were conducted at temperatures at which gas phase O_2 is expected to be depleted under the modulated full feed conditions. The CO oxidation by spinel would also occur

https://doi.org/10.1021/acsengineeringau.3c00053
ACS Eng. Au 2024, 4, 193−203

at the same temperatures. As shown in Figure 8a, a consistent trend was obtained over the 350 to 450 °C temperature range.

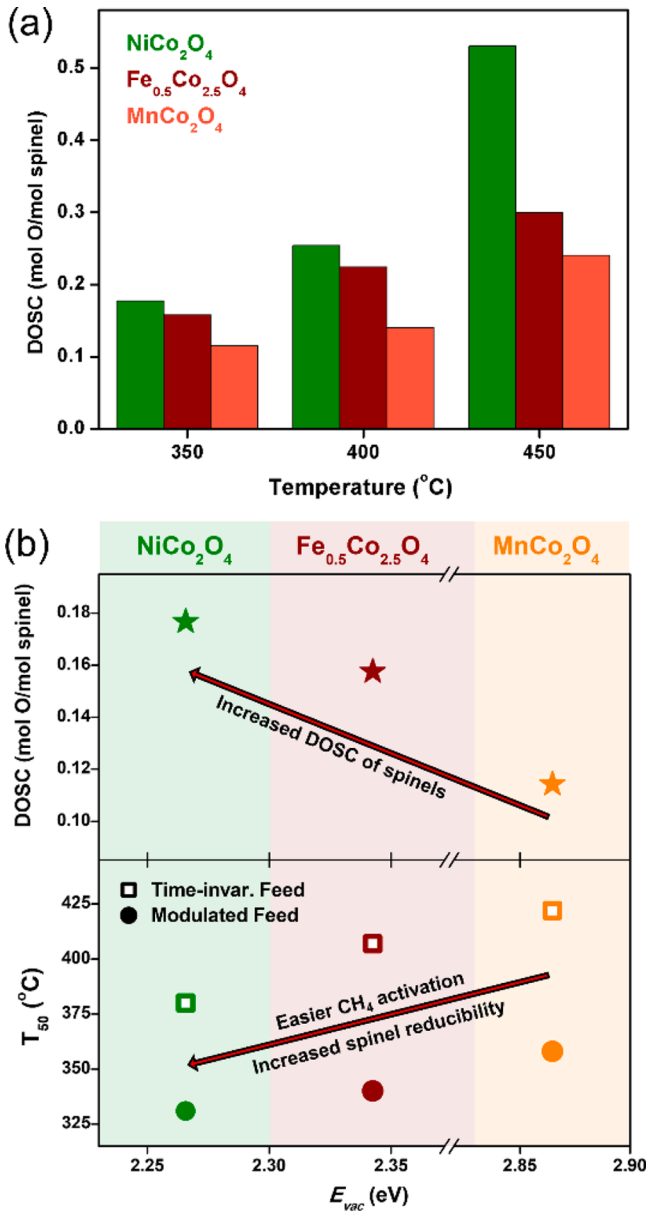

Figure 8. (a) Dynamic oxygen storage capacity quantifications of different spinel oxides; (b) correlation between calculated oxygen vacancy formation energy, E_{vac}, and DOSC at 350 °C (upper panel) and T_{50} for CH_4 light-off (lower panel).

The $NiCo_2O_4$ spinel has the highest DOSC, followed by those of $Fe_{0.5}Co_{2.5}O_4$ and $MnCo_2O_4$. Among these Co-rich spinel samples, $NiCo_2O_4$ provides the lowest CO oxidation temperature, which is expected to be important for enhancing the CH_4 conversion.

Figure 8b shows that the DOSC ranking agrees with the theoretical predictions. To rule out the possibility that the trend is not a result of differences in oxide texture but rather is due to electronic effects, N_2-physisorption (BET) measurements were made of their surface areas. Each of the three cobalt-based samples has comparable surface areas of ∼165 m^2/g (details in Table 4). Their nearly identical values suggest that the DOSC or CO conversion activity of spinel or the indirect CH_4 conversion enhancement is not correlated with the surface area of the samples.

Table 4. Quantified Specific Surface Areas of the Power Spinel Samples

Spinel	Specific surface area (cm^2/g)
$NiCo_2O_4/Al_2O_3$	161.0
$Fe_{0.5}Co_{2.5}O_4/Al_2O_3$	166.5
$MnCo_2O_4/Al_2O_3$	167.7

Several dual-layer PGM+Co-Spinel catalysts were tested for CH_4 conversion. As shown in Figure 9, under both modulated and time-invariant feed conditions, the Co-Spinel containing samples demonstrate methane light-off at lower temperatures than those of the comparable PGM-Only2 sample. The performance order of PGM+Co-Spinel catalysts under both feed conditions in terms of T_{50} is as follows: $NiCo_2O_4$ < $Fe_{0.5}Co_{2.5}O_4$ < $MnCo_2O_4$. Under the time-invariant feed condition, the T_{50} values are 381 °C ($NiCo_2O_4$), 407 °C ($Fe_{0.5}Co_{2.5}O_4$) and 423 °C ($MnCo_2O_4$); under the modulated feed condition, the T_{50} values are 330 °C ($NiCo_2O_4$), 339 °C

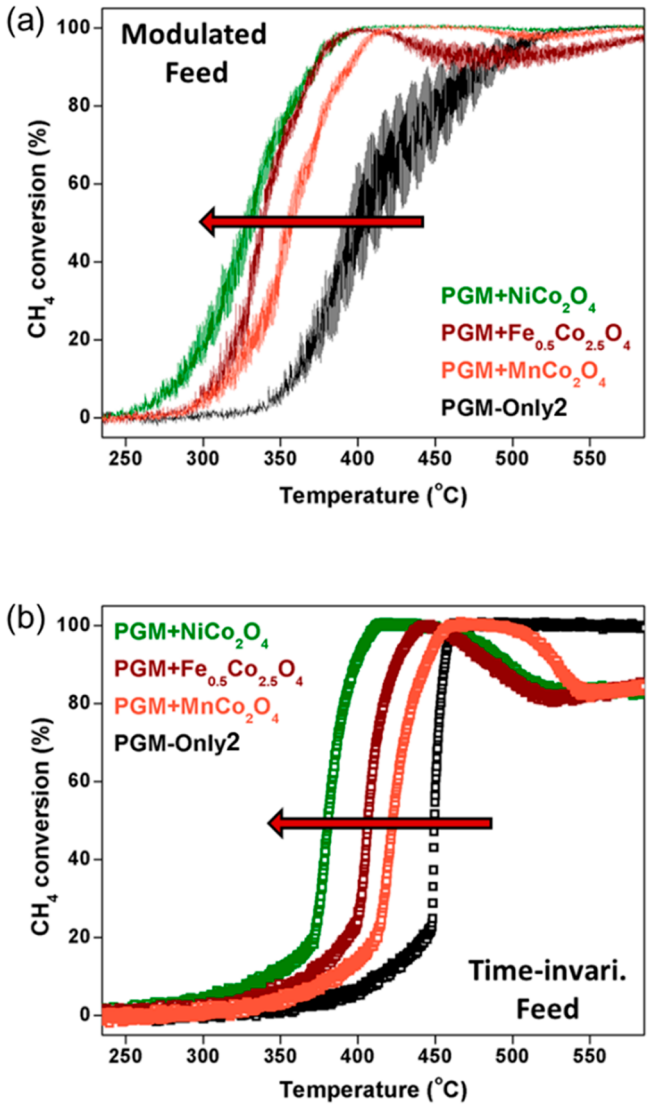

Figure 9. CH_4 conversion (a) under modulated feed and (b) under time-invariant feed.

https://doi.org/10.1021/acsengineeringau.3c00053
ACS Eng. Au 2024, 4, 193−203

($Fe_{0.5}Co_{2.5}O_4$) and 358 °C ($MnCo_2O_4$). Under the time-invariant feed conditions, the PGM+Co-Spinel catalysts failed to achieve full CH_4 conversion at high temperature. A slight decrease in high temperature CH_4 conversion was also observed for the PGM+$Fe_{0.5}Co_{2.5}O_4$ catalyst under modulated feed condition. The drop in CH_4 conversion over the PGM +Spinel catalyst at high temperature has been investigated in an earlier study[6] and discussed in section 3 of the SI. After gas phase O_2 depletes and steam reforming commences at high temperature, the observed activity loss was attributed to base metal and/or metal oxide species migration from the spinel layer to the PGM layer, leading to a loss of active PGM sites. It is noted that the long-term durability and hydrothermal stability of these catalysts at high temperature under net rich condition warrants additional investigations that are outside the scope of this study.

The trend of methane conversion enhancement, as measured by the T_{50} values under both modulated and time-invariant feeds, follows a pattern consistent with that of E_{vac} (Figure 8b) and our DOSC measurements. The agreement suggests that at least for the experimental conditions probed an increased DOSC or dynamic reducibility of the spinel oxides results in a lower CH_4 light-off temperature. For the modulated feed condition, more reactive reductants such as CO and H_2 can be removed by spinel through oxidation with the lattice oxygen under the rich phase; the spinel oxygen vacancies that have formed can be refilled by the excess gas phase oxygen under the lean phase, and then the cycle repeats. With this DOSC function of spinel, the effect of the O_2 inhibition on CH_4 oxidation can be mitigated in part at low methane conversion (before O_2 runs out). As a result, more active PGM sites are available for direct CH_4 oxidation. Under the time-invariant feed condition, DOSC is not needed, but the addition of spinel is still advantageous because it provides catalytic sites for CO and H_2 oxidation. These results corroborate our hypothesis that CH_4 conversion activity over dual-layer PGM catalysts can be enhanced by optimizing the oxygen storage properties of the spinel layer through strategic material composition tuning.

4.4. High-Throughput Reducibility Screening of Ternary Spinel Oxides

While quite successful, the drawbacks of the screening approach summarized in Figure 6 are the need for time-consuming DFT calculations to obtain E_{vac} and B.E.(H) and limiting predictions to synthesizable materials. Stability predictions for ternary oxides are very challenging. While Maiti et al.[40] have previously shown that the heat of formation and bond dissociation energies in binary oxides are correlated with E_{vac}, materials with negative heats of formation may still decompose into other ternary or binary oxide phases. Hence, a complete ternary phase diagram for each composition would be required.

The prediction of E_{vac} and B.E.(H) can be greatly accelerated by bypassing DFT and using tabulated properties as input to empirical models. The essence of material property tuning of transition metal oxides lies in varying the *d* electron content/filling, resulting in variation of the oxidation states of the constituent cations and anions. For this set of spinel oxides, Figure S4a shows the variation of oxygen partial charge as the metal *d* electron content is varied. Oxides with higher *d* electron density or less electropositive metals have oxygen atoms that are less reduced. On the contrary, more electropositive metals in the spinel oxides (having fewer *d* electrons) exhibit a stronger metal−oxygen bond, thus transforming the oxygen to more reduced states. As seen in Figures S4b,c, the reactivity descriptors, E_{vac} and B.E.(H) follow similar trends partial charge on lattice oxygen atoms, imposed by varying metal compositions. And as already showcased in Figure 6, since both B.E.(H) and E_{vac} can be described in unison by the reducibility descriptor E_{vac}, we claim that the search of high-performance spinel oxides as complement to PGMs for CH_4 oxidation catalysts can be conducted by simply counting the *d* electron content of the oxide (Figure 10). This result is an indication that future transition metal oxide screening studies for reducibility purposes or for any reactions closely correlated to the redox properties can be conducted in a first order approximation based on a simple *d* electron content. The screening accuracy can be further improved by building a multivariate model using multiple tabulated properties (atomic radii, electronegativity, etc.), but such model is less likely to maintain physical interpretability.

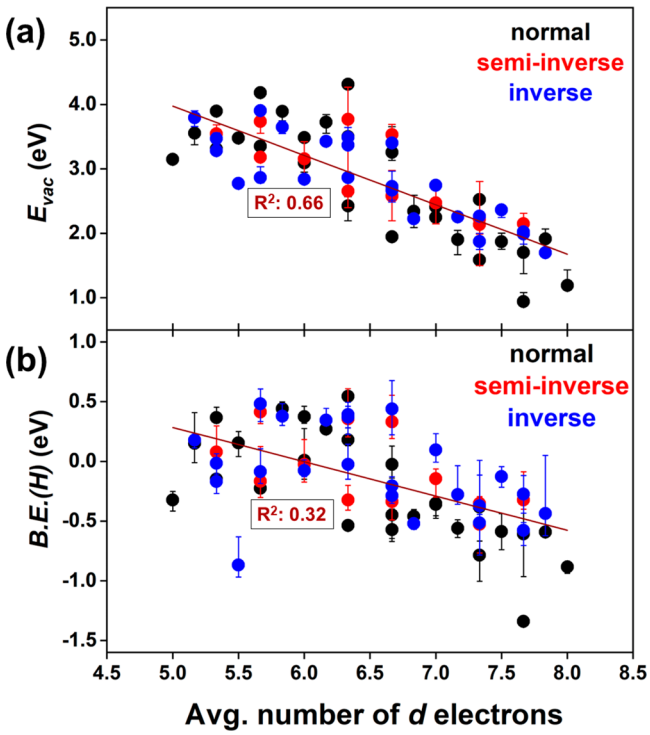

Figure 10. Trends of (a) oxygen vacancy formation energy (E_{vac}) and (b) binding energy of hydrogen (B.E.(H)) over normal, inverse, and semi-inverse phases of spinel oxides having varying *d* electron content ($\sum_i w_i d_i$). Whiskers represent the entire range (min−max) of calculated values.

5. CONCLUSIONS

Dual-layer catalysts consisting of a spinel and PGM layers are efficient in abating methane emissions from natural gas vehicles and engines operated under cyclic lean/rich feed modulation. With the understanding that the beneficial role of a spinel on CH_4 oxidation is dependent on its dynamic oxygen storage capacity (DOSC) and its ability to oxidize intermediates and byproducts, we have systematically screened spinels composed of Mn, Fe, Co, and Ni using their computed oxygen vacancy formation energy (E_{vac}) as descriptor. Density

https://doi.org/10.1021/acsengineeringau.3c00053
ACS Eng. Au 2024, 4, 193−203

functional theory simulations of 64 unique spinels with different composition or inversion identified the family of Co-based spinels as good candidates to work cooperatively with the PGM. To arrive at this subset, we considered the ease of reversible oxygen removal while avoiding over-reduction or high concentrations of Fe and Ni, which are known to form migrating species that can poison active sites on the PGM. Three of the predicted formulations were synthesized, and their spinel crystal structure confirmed with XRD. The measured DOSC of these spinels decreases in the same order as their computed E_{vac}, i.e., $NiCo_2O_4$, > $Fe_{0.5}Co_{2.5}O_4$ > $MnCo_2O_4$. Flow experiments using temperature programs confirmed the correlation between the DOSC of spinel and the catalyst performance in CH_4 conversion under application relevant conditions. Among the tested spinels, $NiCo_2O_4$ shows the highest DOSC and lowest T_{50} of ca. 330 °C, which is 58 °C lower than that of the previously reported $Mn_{0.5}Fe_{2.5}O_4$ spinel under dynamic conditions. Our study demonstrated the effective use of the E_{vac} descriptor in identifying potential spinel candidates, which can be tuned to maximize the dual-layer catalyst efficiency for CH_4 emission control applications. Moreover, we propose that a larger library of spinel oxides can be efficiently screened by counting their *d* electron content. From the broader standpoint of catalyst design for redox chemistries under dynamic reaction conditions, our study makes contributions to developing the critically important ability to design mixed metal oxides with excellent DOSC performance and cyclic stability.

■ ASSOCIATED CONTENT

Supporting Information

The Supporting Information is available free of charge at https://pubs.acs.org/doi/10.1021/acsengineeringau.3c00053.

Measured TPR data over $Mn_{0.5}Fe_{2.5}O_4/Al_2O_3$ sample; methane conversion performance comparison of PGM +Spinel and PGM-Only catalysts with different PGM loadings; steam methane reforming activity of PGM +$NiCo_2O_4$ catalyst; calculated average charge state of lattice oxygen, average oxygen vacancy formation energy, and average binding energy of hydrogen on normal, semi-inverse, and inverse phases of spinel oxides; and formation energies of $MnCo_2O_4$, $Fe_{0.5}Co_{2.5}O_4$, and $NiCo_2O_4$ (PDF)

■ AUTHOR INFORMATION

Corresponding Authors

Lars C. Grabow − *William A Brookshire Department of Chemical and Biomolecular Engineering, University of Houston, Houston, Texas 77204, United States; Texas Center for Superconductivity at the University of Houston (TcSUH), Houston, Texas 77204, United States;* orcid.org/0000-0002-7766-8856; Email: grabow@uh.edu

Michael P. Harold − *William A Brookshire Department of Chemical and Biomolecular Engineering, University of Houston, Houston, Texas 77204, United States;* Email: mpharold@central.uh.edu

Authors

Pak Wing Chen − *William A Brookshire Department of Chemical and Biomolecular Engineering, University of Houston, Houston, Texas 77204, United States;* Present Address: P.W.C.: BASF Environmental Catalyst and Metal Solutions, 25 Middlesex Essex Turnpike, Iselin, New Jersey, 08830, United States; orcid.org/0000-0002-9335-5438

Debtanu Maiti − *William A Brookshire Department of Chemical and Biomolecular Engineering, University of Houston, Houston, Texas 77204, United States;* Present Address: D.M.: Catalysis and Transient Kinetics Group, Idaho National Laboratory, 775 MK Simpson Blvd, Idaho Falls, Idaho, 83401, United States

Ru-Fen Liu − *CDTi Advanced Materials, Inc., Oxnard, California 93033, United States*

Complete contact information is available at: https://pubs.acs.org/10.1021/acsengineeringau.3c00053

Author Contributions

⊥P.W.C. and D.M. contributed equally to this paper. CRediT: **Pak Wing Chen** data curation, formal analysis, investigation, visualization, writing-original draft; **Debtanu Maiti** data curation, formal analysis, investigation, visualization, writing-review & editing; **Ru-Fen Liu** investigation, methodology, resources, writing-review & editing; **Lars C. Grabow** conceptualization, formal analysis, funding acquisition, methodology, resources, software, supervision, writing-review & editing; **Michael P. Harold** conceptualization, formal analysis, funding acquisition, investigation, methodology, project administration, resources, supervision, writing-review & editing.

Notes

The authors declare no competing financial interest.

■ ACKNOWLEDGMENTS

The authors gratefully acknowledge the U.S. Department of Energy (award number: DE-EE0008332) for funding. This research used resources of the National Energy Research Scientific Computing Center (NERSC), a U.S. Department of Energy Office of Science User Facility operated under Contract No. DE- AC02-05CH11231. The authors acknowledge the use of the Opuntia, Sabine, and Carya clusters, and the advanced support from the Research Computing Data Core at the University of Houston to carry out the research presented here.

■ REFERENCES

(1) Huang, F.; Chen, J.; Hu, W.; Li, G.; Wu, Y.; Yuan, S.; Zhong, L.; Chen, Y. Pd or PdO: Catalytic active site of methane oxidation operated close to stoichiometric air-to-fuel for natural gas vehicles. *Appl. Catal., B* **2017**, *219*, 73−81.

(2) Xi, Y.; Ottinger, N.; Liu, Z. G. Development of a Lab Reactor System for the Evaluation of Aftertreatment Catalysts for Stoichiometric Natural Gas Engines. *SAE Technol. Pap.* **2017**, 2017-01-0999.

(3) Heck, R. M.; Farrauto, R. J. Automobile exhaust catalysts. *Appl. Catal., A* **2001**, *221*, 443−457.

(4) Kang, S. B.; Karinshak, K.; Chen, P. W.; Golden, S.; Harold, M. P. Coupled methane and NO_x conversion on Pt + Pd/Al_2O_3 monolith: Conversion enhancement through feed modulation and $Mn_{0.5}Fe_{2.5}O_4$ spinel addition. *Catal. Today* **2021**, *360*, 284−293.

(5) Karinshak, K.; Chen, P. W.; Liu, R.-F.; Golden, S. J.; Harold, M. P. Optimizing feed modulation for coupled methane and NO_x conversion over Pd-Pt/$Mn_{0.5}Fe_{2.5}O_4/Al_2O_3$ monolith catalyst. *Appl. Catal., B* **2022**, *304*, No. 120607.

(6) Chen, P. W.; Maiti, D.; Liu, R.-F.; Grabow, L. C.; Harold, M. P. CH_4 steam reforming on Pt + Pd/Al_2O_3 monolith: impact of

$Mn_{0.5}Fe_{2.5}O_4$ spinel addition. *Catal. Sci. Technol.* **2022**, *12*, 2618−2633.
(7) Golden, S.; Nazarpoor, Z.; Launois, M. Novel Mixed Metal Oxide Structure for Next Generation Three-Way Catalysts. *SAE Technol. Pap.* **2015**, 2015-01-1007.
(8) Heo, I.; Choung, J. W.; Kim, P. S.; Nam, I.-S.; Song, Y. I.; In, C. B.; Yeo, G. K. The alteration of the performance of field-aged Pd-based TWCs towards CO and C_3H_6 oxidation. *Appl. Catal., B* **2009**, *92*, 114−125.
(9) Bickel, J.; Odendall, B.; Eigenberger, G.; Nieken, U. Oxygen storage dominated three-way catalyst modeling for fresh catalysts. *Chem. Eng. Sci.* **2017**, *160*, 34−53.
(10) Yao, H. C.; Yao, Y. F. Ceria in automotive exhaust catalysts: I. Oxygen storage. *J. Catal.* **1984**, *86*, 254−265.
(11) Li, P.; Chen, X.; Li, Y.; Schwank, J. W. A review on oxygen storage capacity of CeO_2-based materials: Influence factors, measurement techniques, and applications in reactions related to catalytic automotive emissions control. *Catal. Today* **2019**, *327*, 90−115.
(12) Zhou, Z.; Harold, M. P.; Luss, D. Enhanced NO, CO and C_3H_6 conversion on Pt/Pd catalysts: Impact of oxygen storage material and catalyst architecture. *Catal. Today* **2021**, *360*, 375−387.
(13) Zhou, Z.; Harold, M. P.; Luss, D. Dynamic Oxygen Storage Capacity of Ceria-Zirconia and $Mn_{0.5}Fe_{2.5}O_4$ Spinel: Experiments and Modeling. *Ind. Eng. Chem. Res.* **2021**, *60*, 6465−6482.
(14) Fino, D.; Russo, N.; Saracco, G.; Specchia, V. CNG engines exhaust gas treatment via Pd-Spinel-type-oxide catalysts. *Catal. Today* **2006**, *117*, 559−563.
(15) Latimer, A. A.; Kulkarni, A. R.; Aljama, H.; Montoya, J. H.; Yoo, J. S.; Tsai, C.; Abild-Pedersen, F.; Studt, F.; Nørskov, J. K. Understanding trends in C−H bond activation in heterogeneous catalysis. *Nat. Mater.* **2017**, *16*, 225−229.
(16) Krcha, M. D.; Mayernick, A. D.; Janik, M. J. Periodic trends of oxygen vacancy formation and C−H bond activation over transition metal-doped CeO_2 (1 1 1) surfaces. *J. Catal.* **2012**, *293*, 103−115.
(17) Yang, Z.; Fu, Z.; Zhang, Y.; Wu, R. Direct CO Oxidation by Lattice Oxygen on Zr-Doped Ceria Surfaces. *Catal. Lett.* **2011**, *141*, 78−82.
(18) Mars, P.; Van Krevelen, D. W. Oxidations carried out by means of vanadium oxide catalysts. *Chem. Eng. Sci.* **1954**, *3*, 41−59.
(19) Kresse, G.; Hafner, J. *Ab initio* molecular dynamics for liquid metals. *Phys. Rev. B* **1993**, *47*, 558−561.
(20) Kresse, G.; Hafner, J. *Ab initio* molecular-dynamics simulation of the liquid-metal−amorphous-semiconductor transition in germanium. *Phys. Rev. B* **1994**, *49*, 14251−14269.
(21) Kresse, G.; Furthmüller, J. Efficiency of ab-initio total energy calculations for metals and semiconductors using a plane-wave basis set. *Comput. Mater. Sci.* **1996**, *6*, 15−50.
(22) Kresse, G.; Furthmüller, J. Efficient iterative schemes for *ab initio* total-energy calculations using a plane-wave basis set. *Phys. Rev. B* **1996**, *54*, 11169−11186.
(23) Kresse, G.; Joubert, D. From ultrasoft pseudopotentials to the projector augmented-wave method. *Phys. Rev. B* **1999**, *59*, 1758−1775.
(24) Wang, L.; Maxisch, T.; Ceder, G. Oxidation energies of transition metal oxides within the GGA + U framework. *Phys. Rev. B* **2006**, *73*, No. 195107.
(25) Wellendorff, J.; Lundgaard, K. T.; Møgelhøj, A.; Petzold, V.; Landis, D. D.; Nørskov, J. K.; Bligaard, T.; Jacobsen, K. W. Density functionals for surface science: Exchange-correlation model development with Bayesian error estimation. *Phys. Rev. B* **2012**, *85*, No. 235149.
(26) Sanville, E.; Kenny, S. D.; Smith, R.; Henkelman, G. Improved grid-based algorithm for Bader charge allocation. *J. Comput. Chem.* **2007**, *28*, 899−908.
(27) Henkelman, G.; Arnaldsson, A.; Jónsson, H. A fast and robust algorithm for Bader decomposition of charge density. *Comput. Mater. Sci.* **2006**, *36*, 354−360.
(28) Chin, Y. H.; Buda, C.; Neurock, M.; Iglesia, E. Reactivity of Chemisorbed Oxygen Atoms and Their Catalytic Consequences during CH_4−O_2 Catalysis on Supported Pt Clusters. *J. Am. Chem. Soc.* **2011**, *133*, 15958−15978.
(29) Becker, E.; Carlsson, P.; Skoglundh, M. Methane Oxidation over Alumina and Ceria Supported Platinum. *Top. Catal.* **2009**, *52*, 1957−1961.
(30) Dickens, C. F.; Montoya, J. H.; Kulkarni, A. R.; Bajdich, M.; Nørskov, J. K. An electronic structure descriptor for oxygen reactivity at metal and metal-oxide surfaces. *Surf. Sci.* **2019**, *681*, 122−129.
(31) Maiti, D.; Daza, Y. A.; Yung, M. M.; Kuhn, J. N.; Bhethanabotla, V. R. Oxygen vacancy formation characteristics in the bulk and across different surface terminations of $La_{(1-x)}Sr_xFe_{(1-y)}Co_yO_{(3-\delta)}$ perovskite oxides for CO_2 conversion. *J. Mater. Chem. A* **2016**, *4*, 5137−5148.
(32) Singh, S.; Pramanik, P.; Sangaraju, S.; Mallick, A.; Giebeler, L.; Thota, S. Size-dependent structural, magnetic, and optical properties of $MnCo_2O_4$ nanocrystallites. *J. Appl. Phys.* **2017**, *121*, No. 194303.
(33) Walsh, A.; Wei, S.-H.; Yan, Y.; Al-Jassim, M. M.; Turner, J. A.; Woodhouse, M.; Parkinson, B. A. Structural, magnetic, and electronic properties of the Co-Fe-Al oxide spinel system: Density-functional theory calculations. *Phys. Rev. B* **2007**, *76*, No. 165119.
(34) Zhang, R.; Liu, M.; Liu, W.; Wang, H. Highly conductive n-type $NiCo_2O_{4-\delta}$ epitaxial thin films grown by RF sputtering. *Mater. Lett.* **2017**, *199*, 164−167.
(35) Dho, J.; Kim, J. Magnetic domain structure of the ferrimagnetic (001) $NiCo_2O_4$ film with perpendicular magnetic anisotropy. *Thin Solid Films* **2022**, *756*, No. 139361.
(36) Kang, S.; Mo, Y.; Ong, S. P.; Ceder, G. Nanoscale Stabilization of Sodium Oxides: Implications for Na−O_2 Batteries. *Nano Lett.* **2014**, *14*, 1016−1020.
(37) Jain, A.; Ong, S. P.; Hautier, G.; Chen, W.; Richards, W. D.; Dacek, S.; Cholia, S.; Gunter, D.; Skinner, D.; Ceder, G.; Persson, K. A. Commentary: The Materials Project: A materials genome approach to accelerating materials innovation. *APL Mater.* **2013**, *1*, No. 011002.
(38) Descorme, C.; Taha, R.; Mouaddib-Moral, N.; Duprez, D. Oxygen storage capacity measurements of three-way catalysts under transient conditions. *Appl. Catal., A* **2002**, *223*, 287−299.
(39) Hickey, N.; Fornasiero, P.; Di Monte, R.; Kaspar, J.; Graziani, M.; Dolcetti, G. A comparative study of oxygen storage capacity over $Ce_{0.6}Zr_{0.4}O_2$ mixed oxides investigated by temperature-programmed reduction and dynamic OSC measurements. *Catal. Lett.* **2001**, *72*, 45−50.
(40) Maiti, D.; Hare, B. J.; Daza, Y. A.; Ramos, A. E.; Kuhn, J. N.; Bhethanabotla, V. R. Earth abundant perovskite oxides for low temperature CO_2 conversion. *Energy Environ. Sci.* **2018**, *11*, 648−659.

https://doi.org/10.1021/acsengineeringau.3c00053
ACS Eng. Au 2024, 4, 193−203